Transactions in Optics and Photonics
https://ojs.wiserpub.com/index.php/TOP/

Research Article

Improving the Photon-Electron Coupling Efficiency in GaN-Based Square Microdisks

Jing Zhou[1], Zili Xie[2], Xiangqian Xiu[2], Dunjun Chen[2], Yi Shi[2], Rong Zhang[2], Youdou Zheng[2], Peng Chen[3]*

[1] School of Integrated Circuits, Anhui University, Anhui, Hefei, 230000, China
[2] School of Electronic Science and Engineering, Jiangsu Provincial Key Laboratory of Advanced Photonic and Electronic Materials, Nanjing University, Jiangsu, Nanjing, 210093, China
[3] Key Laboratory of Advanced Photonic and Electronic Materials, School of Electronic Science and Engineering, Nanjing University, 163 Xianlin Road, Nanjing, 210023, China
E-mail: pchen@nju.edu.cn

Received: 16 June 2025; **Revised:** 23 July 2025; **Accepted:** 29 July 2025

Abstract: In this work, two types of GaN-based square microdisks, which are suspended microdisks and microdisks with a porous bottom layer based on standard blue/green Light-Emitting Diode (LED) structures grown on Si substrates, are studied. At room temperature, resonant emission was observed in the suspended square microdisk, and the porous microdisk achieved optically pumped lasing at a wavelength of 479 nm with a threshold of 4.37 mW. Optical field simulations reveal that the bridges of the suspended microdisk not only facilitate the transport of light from the microdisk into the bridges for directed propagation but also have no impact on the internal light field distribution. On the other hand, the lasing results of the microdisks with the porous bottom layer demonstrate that the presence of the porous layer enables a high degree of photon confinement within the active region. The results from both types of microdisks confirm that the electron-photon coupling efficiency can be significantly enhanced in the square microcavities, and furthermore that the optical signals can be effectively transmitted through the bridges of the suspended microdisks. This work presents a highly promising approach for Si-based optoelectronic integration.

Keywords: GaN, microdisk, lasing, electron-photon coupling

Abbreviation

WGM	Whispering-Gallery Mode
LED	Light Emitting Diode
MQWs	Multiple Quantum Wells
PECVD	Plasma-Enhanced Chemical Vapor Deposition
ICP	Inductively Coupled Plasma
BOE	Buffered Oxide Etching
SEM	Scanning Electronic Microscopy

DOI:

CW	Continuous-Wave
PL	Photo Luminescence
FDTD	Finite Difference Time Domain
FWHM	Full Width Half Maximum

1. Introduction

Due to the maturity and cost-effectiveness of silicon-based technologies, silicon-based optoelectronic devices are ideal on-chip light sources for integrating electronics and photonics. Silicon-based laser diodes hold great potential as on-chip light sources, meeting the demands for manufacturing photonic-electronic integrated circuits essential for communications and computing technologies [1–3].

In recent years, substantial research has been conducted into various laser diode geometries, and the microdisk laser featuring Whispering-Gallery Modes (WGM) stands out due to its high-quality factor (Q) and low threshold [4–6]. Group III nitrides are typical direct bandgap semiconductors with a wide range of bandgap energies, spanning from 0.7 eV to 6.2 eV [7–9]. Among them, GaN is notable for its exceptional ability to emit blue light. To reduce defect density, it is essential to grow thick epitaxial layers, as there is a significant potential for defects to form at the interface between the GaN epitaxial layer and the silicon substrate [10, 11]. However, microdisks thicker than λ/n introduce longitudinal modes that decrease the photon-electron coupling efficiency of the microdisks [12]. Additionally, light absorption by the silicon substrate cannot be overlooked. This presents a significant challenge for achieving silicon-based microdisk lasers with effective optical confinement.

Most reported GaN-on-Si microdisks are undercut structures, in which the silicon substrate is wet-etched to the point where the microdisk is supported solely by the underlying post [13–15]. Undercut microdisks do not fully optimize photon confinement in the active region, and there is a significant likelihood of light field leakage from the supporting silicon posts. Moreover, achieving electrically pumped lasing in undercut microdisks with a silicon substrate is extremely rare. The requirement to fabricate the *n*-electrode on the silicon substrate complicates current flow due to the presence of a non-doped, high-resistance AlN/AlGaN buffer layer between the silicon and GaN. Additionally, the narrow pillar of the microdisk introduces considerable thermal resistance, which can diminish both the device's lifespan and lasing efficiency [16].

This study tackles the issue of low photon-electron coupling efficiency in thick microdisks by introducing two easily fabricated designs. The first design is a suspended microdisk supported by two straight bridges. The second design features the microdisk with a porous bottom layer, where the highly doped *n*-GaN layer within the microdisk is transformed into a porous structure. Experimental findings demonstrate that both types of microdisks effectively confine photons within the active region, thereby enhancing the photon-electron coupling efficiency of the microdisks.

2. Experiment

A square suspended microdisk with a side length of 8.5 μm was fabricated using a standard blue Light-Emitting-Diode (LED) wafer grown on a silicon (111) substrate. The epitaxial structure of the wafer, as shown in Figure 1a, consists of an AlN/AlGaN buffer layer (1.5 μm thick), a 1.5 μm *n*-GaN layer, six pairs of InGaN/GaN Multiple Quantum Wells (MQWs) with emission in the blue range, and a 200 nm p-GaN layer, resulting in a total thickness of approximately 3.3 μm. The use of a standard LED epitaxial wafer facilitates progress toward electrically pumped lasing and commercial applications.

The epitaxial wafer used in the microdisks with a porous bottom layer differs from that of the suspended microdisk, as illustrated in Figure 1b. Specifically, a 1-μm-thick *n*+ GaN layer and a 100-nm *u*-GaN layer are inserted between the *n*-GaN layer and the MQWs emission in the green range. During the fabrication process, electrochemical etching is applied to transform the *n*+ GaN layer into a porous layer. The *u*-GaN layer, grown atop the *n*+ GaN layer, serves as a protective barrier, shielding the MQWs active region from potential damage caused by the etching process.

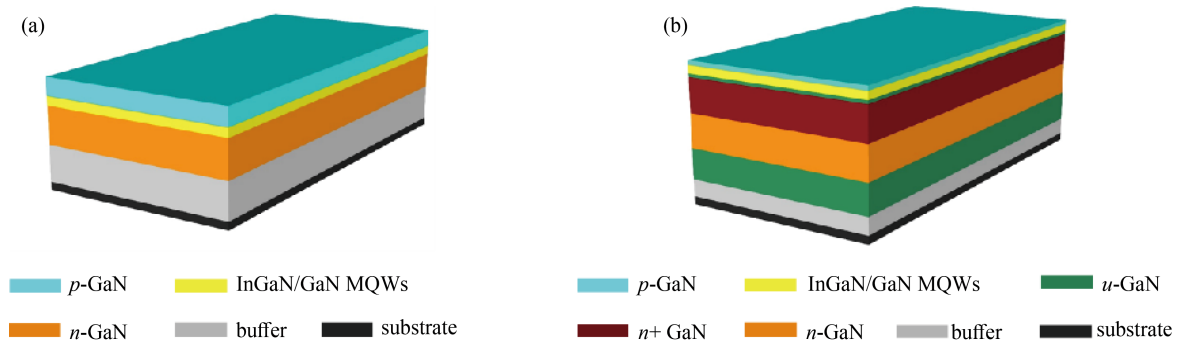

Figure 1. Epitaxial wafer structures for the (a) suspended microdisks wafer and (b) porous microdisks wafer

The suspended microdisk design features two diagonal bridges, each 15 μm long and 1.5 μm wide, that support the microdisk after the part of the silicon has been etched away. First, a 200 nm SiO_2 film was deposited onto the wafer using Plasma-Enhanced Chemical Vapor Deposition (PECVD). The square microcavity pattern with the bridges was then transferred onto a photoresist layer via lithography. Using the photoresist as a mask, the SiO_2 layer was etched in a reactive ion etching system. Subsequently, the GaN epitaxial layer was etched down to the Si surface by using an Inductively Coupled Plasma (ICP) dry etching system with BCl_3 and Cl_2 plasma. Finally, isotropic wet etching with an HNO_3, HF, and H_2O solution was employed to remove part of the silicon substrate, leaving the microdisk suspended by its supporting bridges, as shown in Figure 2.

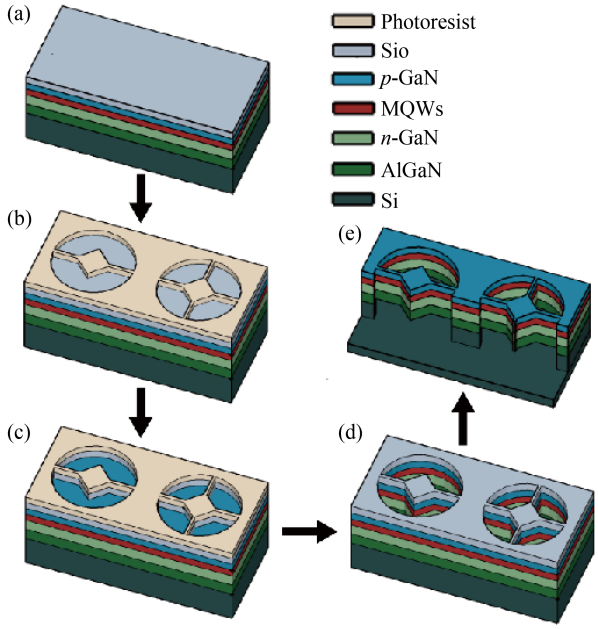

Figure 2. Fabrication process of the square microdisk with bridges. (a) Deposition of SiO_2, (b) Photolithography, (c) Reactive ion etching of the SiO_2 layer, (d) ICP etching of the GaN epitaxial layer, (e) Isotropic wet etching of the silicon substrate

The fabrication process for microdisks with a porous bottom layer differs after the ICP etching of the GaN epitaxial layer down to the *n*-GaN layer. The final step involves electrochemical etching to convert the *n*+ GaN layer to the porous layer [17, 18]. The etching solution consists of a mixture of oxalic acid and phosphoric acid. The wafer serves as the anode, while a Platinum (Pt) chip acts as the cathode. The applied voltage varies slightly depending on the size of the

microdisk, typically ranging from 15 to 20 V. After the electrochemical etching process, a Buffered Oxide Etching (BOE) solution is used to remove the SiO_2 layer from the surface of the sample.

The morphology of the microdisks is observed by Scanning Electron Microscopy (SEM). Optical properties are measured by photoluminescence at room temperature.

3. Results and discussion

The SEM image of the suspended square microdisks with two and four bridges is presented in Figure 3. The microdisks exhibit smooth morphology on both the top surface and the sidewalls, which helps facilitate effective confinement of optical modes within the microdisks. Since the silicon substrate beneath the microdisk is completely etched away, this design provides three-dimensional optical confinement. Without light leakage through the underlying silicon pillar, the optical confinement within the microdisk is significantly enhanced. Compared to the normal undercut microdisks, this approach minimizes optical losses. This improved confinement leads to better photo-coupling efficiency, as the optical modes are more effectively contained within the microdisk, reducing losses and optimizing performance. Of course, more bridge connections will lead to more light exits and will also affect the internal modes. So, the number of bridges is limited and should be determined by minimum connection requirements.

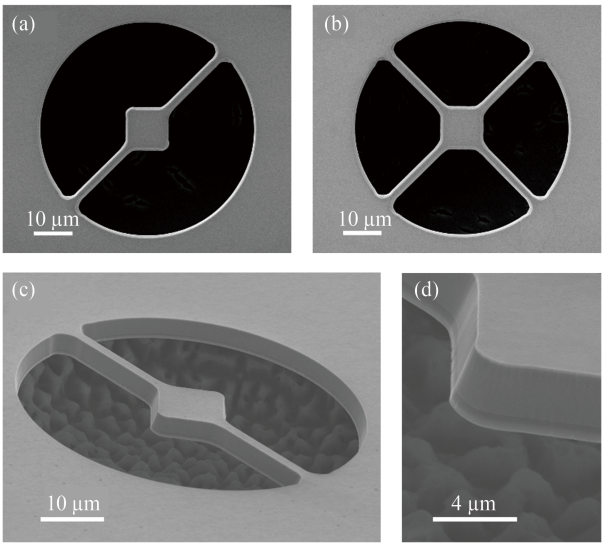

Figure 3. Top view of SEM images of suspended microdisk with two bridges (a) and four bridges (b). Tilted view of SEM images of a suspended microdisk with two bridges (c). Zoom-in tilted view of sidewalls of the suspended microdisk (d)

Figure 4a shows square porous microdisks with a side length of 6 μm; the inset is a top view. A square microdisk with round corners is beneficial to achieve single-mode emission [19]. The sidewalls of the microdisk are very vertical and the porous structure in the middle layer is clearly visible, which is crucial to achieving high performance of lasing later. The *n*+ GaN layer has been completely converted into the porous layer with an average pore diameter of around 40 nm.

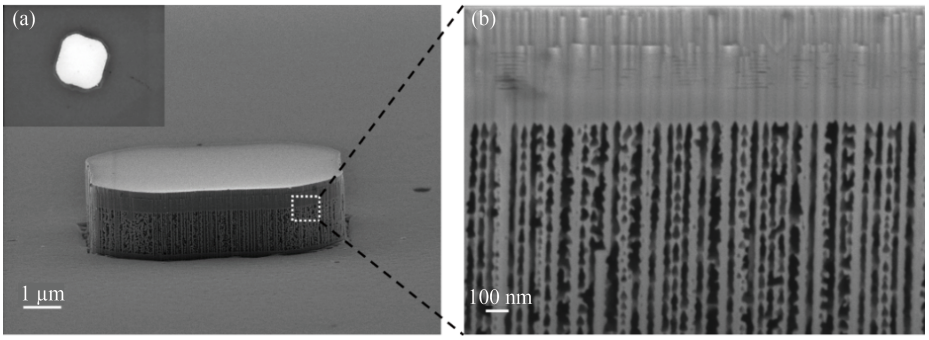

Figure 4. SEM images of square porous microdisk with side length of 6 μm, the inset is top view (a), and zoom-in view of the sidewall with the porous structure (b)

The optical characteristics of the suspended microdisks were measured under a Continuous-Wave (CW) 375 nm laser at room temperature. The luminescence signals were collected using a Horiba iHR320 monochromator and detected by a Synapse CCD detector. Figure 5 presents the Photo Luminescence (PL) spectra of the suspended microdisks with two bridges as a function of pump power. At relatively low pump power, the spontaneous emission peak centered around 445 nm spans a broad wavelength range. As the pump power increases, the spontaneous emission peak exhibits a blue shift to centered around 440 nm. This blue shift is likely caused by increased carrier densities within the microdisk, which result in band-filling effects. Such behavior is frequently observed in optoelectronic devices as the excitation power increases.

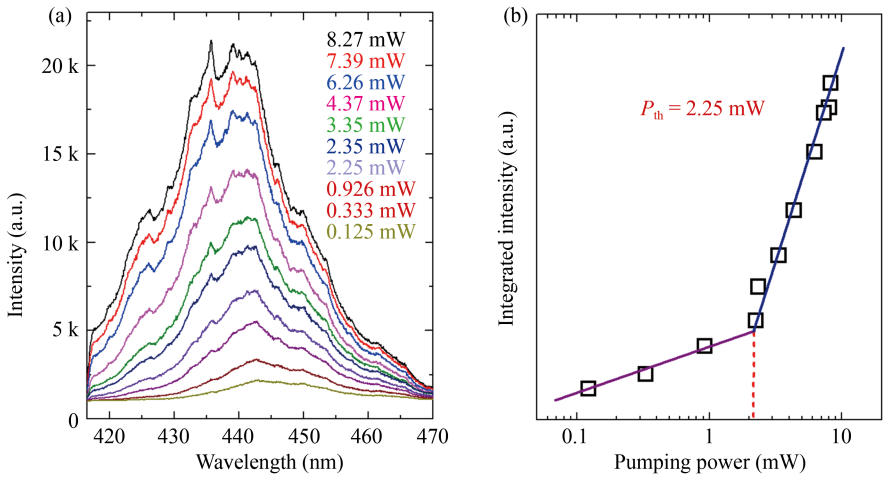

Figure 5. PL spectra (a) and the integrated PL spectra intensity versus pump optical power of suspended microdisks with two bridges (b)

However, upon closely examining the PL spectra at high pump power, a series of sharp peaks can be observed, superimposed on the broad spontaneous emission curve. Meanwhile, the wavelengths of these small emission peaks remain stable, especially for the sharp peak at 436 nm. The stability of the emission peak positions is indeed a key characteristic of resonant emission. Furthermore, the relationship between pump power and integrated intensity is shown in Figure 5b, where the curve displays a distinct kink, confirming the transition from spontaneous emission to partially resonant emission. This transition occurs at a threshold power of 2.25 mW under room-temperature conditions.

The microdisk did not exhibit clear laser action, possibly because it was not driven strongly enough. The heating effect at high CW pump power limits any further increase in output power [20]. However, the more significant reason is that the suspended microdisks fabricated from a standard LED wafer are significantly thicker than λ/n. A thicker microdisk leads to two serious consequences. First, it results in the formation of multiple longitudinal modes, causing the

energy of all optical modes not overlapping with the MQW to be wasted, preventing electron-photon coupling. Second, the sidewalls of the thick disk exhibit an inclination angle, as shown in Figure 3d. This inclined sidewall further disrupts the coupling between the optical modes and the top quantum well, a finding already reported in our previous research [12]. Therefore, excessive microdisk thickness leads to huge optical losses and more pronounced impurity absorption [19].

Although only a portion of the emission transitions to resonant emission, the bridge structure can still contribute to the optical output characteristics. The electric field distributions of the microdisks with two bridges are simulated using 2-Dimensional Finite Difference Time Domain (2D-FDTD). As TM-polarized emission is significantly weaker than TE-polarized emission in the GaN material system, only the characteristics of the TE mode are analyzed. Dipoles are positioned within the active region to excite the WGMs inside the GaN microdisk. The monitoring plane is placed in the axial section to observe the electric field distribution within the microdisk.

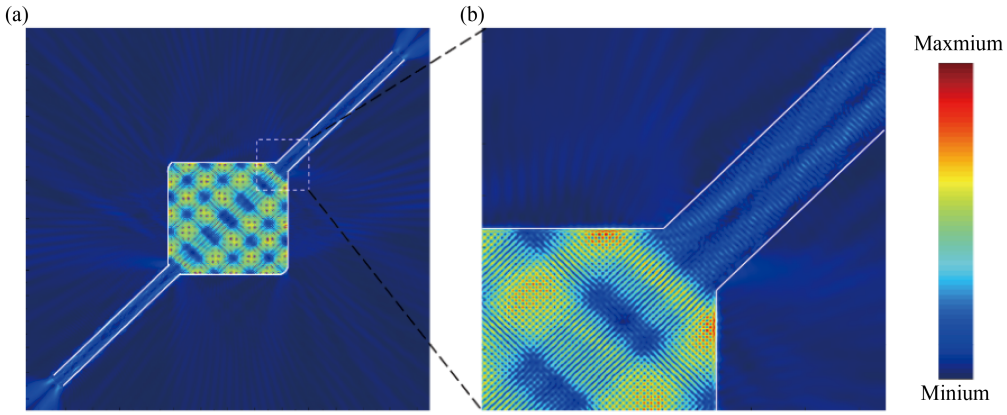

Figure 6. Electric field distributions of optical modes with highest Q factor in the suspended microdisks with two bridges (a) and Zoom in: enlarged view for corresponding mode field distributions in the connection regions (b)

From Figure 6a, similar to circular microdisks, WGMs can also be realized within square microcavities. The key difference lies in the light propagation paths: in square microcavities, the paths are confined to regular and discrete orbits, which facilitates mode control and selection. More importantly, the modes in square microcavities are uniformly distributed throughout the cavity, unlike in circular microcavities, where the modes are predominantly concentrated at the boundaries. As a result, the bridges extending from the corners of the square microcavities do not disrupt the light field distribution within the cavity.

Although the corner-connected bridges do not disrupt the light resonance paths within the disk, the resonant emission inside the disk can still be coupled into the bridge structure. The zoomed-in image, Figure 6b, shows that the mode field is efficiently coupled into the bridges. Unlike the nondirectional light scattering commonly observed at rounded corners, a clearly unidirectional emission propagating along the bridges is evident. This indicates that the straight bridges directly connected to square microcavities can serve as output waveguides, delivering highly unidirectional emission. These suspended microcavities with straight bridges present significant potential for applications in optical interconnects and photonic integration.

As discussed above, the suspended microdisk has a thickness greater than λ/n, leading to higher optical losses, particularly in the longitudinal direction. To address this, the microdisks with a porous bottom layer can offer effective longitudinal optical confinement. We have reported the model for the porous layer [21], in which the porous layer is defined as composed of air cylinders with a diameter of D_{pore}, and an interval of d, and $D_{pore} + d \approx 55$ nm. The porosity φ_{pore} of microdisks can be changed by varying the D_{pore}.

$$\varphi_{pore} = \pi {D_{pore}}^{2/2} 4 (D_{pore} + d)^2 \tag{1}$$

When D_{pore} = 40 nm, the porosity pore is 42%.

As the porosity increases, there is a constant drop in the refractive index of the porous layer, further restricting light from entering these low-refractive-index regions, confining it to the upper high-refractive-index MQW region. When pore is greater than 40%, there is essentially little optical field distribution in the porous area [21]. Thus, with the increase of porosity, the refractive index difference between the MQW region and the other regions increases, which improves the light confinement in the active region, and then this can improve the photon-electron coupling efficiency in the microdisks, even leading to lasing at room temperature.

Furthermore, beyond the advantages of light confinement, the porous layer also offers benefits for device heat dissipation. Previously, realizing WGM microdisk structures typically involved undercut mushroom-shaped designs [12–15]. This resulted in a very narrow heat dissipation pathway through the central pillar, making efficient heat removal extremely challenging. Although porous GaN has lower thermal conductivity than fully solid GaN, it still exhibits relatively good thermal conductivity, and other groups' experimental work has demonstrated its suitability for laser applications [22]. In this work, the fabricated porous layer replaces the air gap beneath the previous device designs for light confinement. The porous layer remains a solid connection to the substrate, providing both an effective heat dissipation pathway and a good electrical conduction pathway, significantly advantageous for future electrical injection, representing another key advantage of our porous layer microdisk structure.

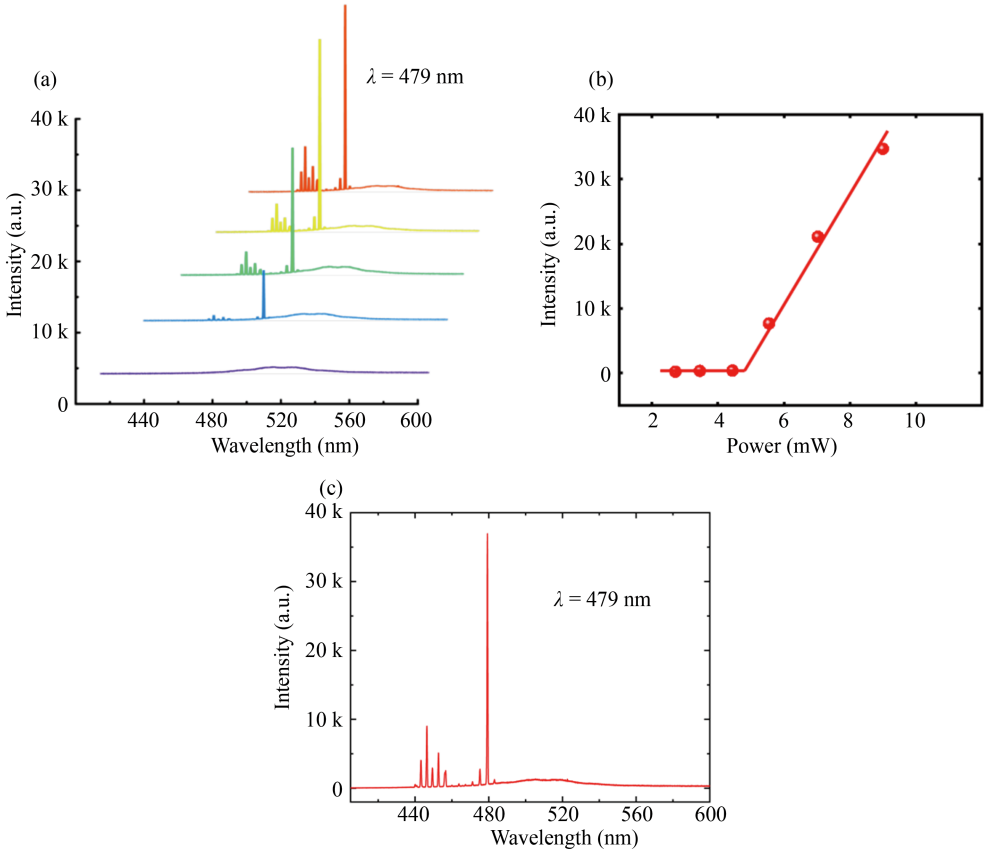

Figure 7. Photoluminescence spectra of microdisks with side length L = 6 μm (a), the peak intensity versus pump power for the square microdisk (b) and the spectrum under the highest excitation (c)

The microdisks with a porous bottom layer were measured by another PL setup at room temperature. The excitation light source is a Mira900F femtosecond laser, the laser wavelength, pulse width, and frequency are set to 375 nm, 140 fs, and 76 MHz, respectively. The light spot is focused and completely covers the microdisk. Figure 7a is the PL spectra

of the square microdisk with a porous bottom layer at room temperature. At low pump power, the microdisk exhibits a wide spectrum of spontaneous emission. With the increase of pump power, several sharp emission peaks appear on the microdisk. The strongest emission peaks of Figure 7a are 479 nm, and the Full Width at Half Maximum (FWHM) is 0.35 nm. The quality factor Q of the main emission peak is defined as $Q = \lambda / \Delta\lambda$, where λ and $\Delta\lambda$ represent the center wavelength and FWHM of the emission peak. The Q value is 1,369. The plot of peak intensity with pump power is shown in figure 7b. The appearance of the kink proves the transition from spontaneous emission to lasing in the microdisk. The threshold is defined as the power at the kink, and the thresholds of the microdisks are 4.37 mW. To more clearly show the lasing peaks, the spectrum under the highest excitation is shown in Figure 7c.

4. Conclusion

Using the standard blue/green LED wafers, two types of square microdisks have been fabricated. One is the suspended microdisk with bridges, which can significantly enhance light confinement within the microcavities due to the high refractive index contrast with air. Simulation results indicate that the bridges can serve as an output waveguide. Another one is the square microdisks with a porous bottom layer, which can achieve optically pumped lasing at room temperature with a threshold power of 4.37 mW and a Q factor of 1,369. These results reveal that the porous layer greatly improves photon confinement in the active region, thereby enhancing photon-electron coupling efficiency within the microdisks. Furthermore, the bridging structure of the suspended microdisk demonstrated the efficient transmission of optical signals through the bridge. The further concept can be the novel microdisk lasers by integrating suspended square microdisks with the porous structures. This approach provides a novel strategy for directional optical waveguide devices.

Funding

This work is supported by National Key Research and Development Program of China (2024YFE0204600).

Author contributions

Conceptualization: Chen P.
Formal analysis: Zhou J.
Methodology: Zhou J, Xie Z, Xiu X and Chen D.
Software: Zhou J.
Investigation: Zhou J. and Chen P.
Resources: Chen P.
Data curation: Zhou J.
Writing-original draft preparation: Zhou J.
Writing-review and editing: Chen P.
Supervision: Shi Y, Zhang R and Zheng Y.
Project administration: Chen P.
Funding acquisition: Chen P.
All authors read and approved the final manuscript.

Conflict of interest

The authors declare no competing financial interest.

References

[1] Zhou Z, Yin B, Michel J. On-chip light sources for silicon photonics. *Light: Science Applications*. 2015; 4(4): e358. Available from: https://doi.org/10.1038/lsa.2015.131.

[2] Han Y, Park H, Bowers J, Lau KM. Recent advances in light sources on silicon. *Advances in Optics and Photonics*. 2022; 14(3): 404-454. Available from: https://doi.org/10.1364/AOP.455976.

[3] Tang M, Park JS, Wang Z, Chen S, Jurczak P, Seeds A, et al. Integration of III-V lasers on Si for Si photonics. *Progress in Quantum Electronics*. 2019; 66: 1-18. Available from: https://doi.org/10.1016/j.pquantelec.2019.05.002.

[4] Kersuzan C, Celaj S, Daney de Marcillac W, Pons T, Maître AS. Photolithographed whispering gallery mode microdisk cavities coupled to semiconductor quantum dots. *ACS Photonics*. 2024; 11(4): 1715-1723. Available from: https://doi/10.1021/acsphotonics.4c00023.

[5] Wang Z, Cheung YF, Fu WY, Choi HW. Enhancing optical confinement of InGaN thin-film microdisk lasers with hybrid omnidirectional reflectors. *ACS Photonics*. 2024; 11(5): 1990-1997. Available from: https://doi/10.1021/acsphotonics.4c00132.

[6] Chen B, Wu S, Ren Y, Wang X, Wei D, Liu J. Nonlinear photon generations from subwavelength whispering-gallery-mode resonator. *Nano Letters*. 2024; 24(24): 7467-7473. Available from: https://doi/10.1021/acs.nanolett.4c01730.

[7] Wu J. When group-III nitrides go infrared: New properties and perspectives. *Journal of Applied Physics*. 2009; 106: 011101. Available from: https://doi.org/10.1063/1.3155798.

[8] Mohammad SN, Morkoç H. Progress and prospects of group-III nitride semiconductors. *Progress in Quantum Electronics*. 1996; 20(5-6): 361-525. Available from: https://doi.org/10.1016/S0079-6727(96)00002-X.

[9] Chen F, Ji X, Lau SP. Recent progress in group III-nitride nanostructures: From materials to applications. *Materials Science and Engineering: R: Reports*. 2020; 142: 100578. Available from: https://doi.org/10.1016/j.mser.2020.100578.

[10] Nakada Y, Aksenov I, Okumura H. GaN heteroepitaxial growth on silicon nitride buffer layers formed on Si (111) surfaces by plasma-assisted molecular beam epitaxy. *Applied Physics Letters*. 1998; 73: 827-829. Available from: https://doi.org/10.1063/1.122014.

[11] Reiher A, Bläsing J, Dadgar A, Diez A, Krost A. Efficient stress relief in GaN heteroepitaxy on Si (111) using low-temperature AlN interlayers. *Journal of Crystal Growth*. 2003; 248: 563-567. Available from: https://doi.org/10.1016/S0022-0248(02)01880-8.

[12] Liu M, Chen P, Xie Z, Xiu X, Chen D, Liu B, et al. High-efficiency photon–electron coupling resonant emission in GaN-based microdisks on Si. *Chinese Physics B*. 2020; 29(8): 084203. Available from: https://doi.org/10.1088/1674-1056/ab9443.

[13] Choi H, Hui K, Lai P, Chen P, Zhang X, Tripathy S, et al. Lasing in GaN microdisks pivoted on Si. *Applied Physics Letters*. 2006; 89: 211101. Available from: https://doi.org/10.1063/1.2392673.

[14] Selles J, Crepel V, Roland I, El Kurdi M, Checoury X, Boucaud P, et al. III-Nitride-on-silicon microdisk lasers from the blue to the deep ultra-violet. *Applied Physics Letters*. 2016; 109: 231101. Available from: https://doi.org/10.1063/1.4971357.

[15] Kouno T, Sakai M, Kishino K, Hara K. Optical microresonant modes acting in thin hexagonal GaN microdisk. *Japanese Journal of Applied Physics*. 2014; 53: 072001. Available from: http://dx.doi.org/10.7567/JJAP.53.072001.

[16] Thiyagarajan S, Levi A, Lin C, Kim I, Dapkus P, Pearton S. Continuous room-temperature operation of optically pumped InGaAs/InGaAsP microdisk lasers. *Electronics Letters*. 1998; 34(24): 2333-2334. Available from: https://doi.org/10.1049/el:19981639.

[17] Zhang C, Park SH, Chen D, Lin DW, Xiong W, Kuo HC, et al. Mesoporous GaN for photonic engineering highly reflective GaN mirrors as an example. *ACS Photonics*. 2015; 2(7): 980-986. Available from: https://doi.org/10.1021/acsphotonics.5b00216.

[18] Zhang Y, Sun Q, Leung B, Simon J, Lee ML, Han J. The fabrication of large-area, free-standing GaN by a novel nanoetching process. *Nanotechnology*. 2010; 22: 045603. Available from: http://dx.doi.org/10.1088/0957-4484/22/4/045603.

[19] Liu M, Chen P, Xie Z, Xiu X, Chen D, Liu B, et al. Approach to single-mode dominated resonant emission in GaN-based square microdisks on Si. *Chinese Physics Letters*. 2020; 37(5): 054204. Available from: https://doi.org/10.1088/0256-307X/37/5/054204.

[20] Stange D, Wirths S, Geiger R, Schulte-Braucks C, Marzban B, Von Den Driesch N, et al. Optically pumped GeSn microdisk lasers on Si. *ACS Photonics*. 2016; 3(7): 1279-1285. Available from: https://doi.org/10.1021/acsphotonics.6b00258.

[21] Li Y, Zhou J, Yan Z, Zhang X, Xie Z, Xiu X, et al. GaN microdisks with a single porous optical confinement layer for whispering gallery mode lasing. *Applied Physics Letters*. 2024; 125: 093504. Available from: https://dx.doi.org/10.1063/5.0223245.

[22] Anderson R, Cohen D, Zhang H, Trageser E, Palmquist N, Nakamura S, et al. Nano-porous GaN cladding and scattering loss in edge emitting laser diodes. *Optics Express*. 2022; 30(2): 2759-2767. Available from: https://doi.org/10.1364/oe.445512.